PLOS | ONE

RESEARCH ARTICLE

15-Deoxy-$\Delta^{12,14}$-Prostaglandin J_2 Inhibits Osteolytic Breast Cancer Bone Metastasis and Estrogen Deficiency-Induced Bone Loss

Ki Rim Kim[1,2], Hyun Jeong Kim[2,3], Sun Kyoung Lee[2,3], Gwang Taek Ma[3], Kwang Kyun Park[2,3], Won Yoon Chung[2,3]*

1 Department of Dental Hygiene, Kyungpook National University, Sangju, 742–711, Korea, **2** Department of Oral Biology, Oral Cancer Research Institute, BK21 PLUS project, Yonsei University College of Dentistry, Seoul, 120–752, Korea, **3** Department of Applied Life Science, The Graduate School, Yonsei University, Seoul, 120–749, Korea

* wychung@yuhs.ac

Citation: Kim KR, Kim HJ, Lee SK, Ma GT, Park KK, Chung WY (2015) 15-Deoxy-$\Delta^{12,14}$-Prostaglandin J_2 Inhibits Osteolytic Breast Cancer Bone Metastasis and Estrogen Deficiency-Induced Bone Loss. PLoS ONE 10(4): e0122764. doi:10.1371/journal.pone.0122764

Academic Editor: Dominique Heymann, Faculté de médecine de Nantes, FRANCE

Received: November 18, 2014

Accepted: February 13, 2015

Published: April 10, 2015

Data Availability Statement: All relevant data are within the paper.

Funding: This work was supported by a faculty research grant from Yonsei University College of Dentistry for 2009 (6-2009-0025). The funders had no role in study design, data collection and analysis, decision to publish, or preparation of the manuscript.

Competing Interests: The authors have declared that no competing interests exist.

Abstract

Breast cancer is the major cause of cancer death in women worldwide. The most common site of metastasis is bone. Bone metastases obstruct the normal bone remodeling process and aberrantly enhance osteoclast-mediated bone resorption, which results in osteolytic lesions. 15-deoxy-$\Delta^{12,14}$-prostaglandin J_2 (15d-PGJ_2) is an endogenous ligand of peroxisome proliferator-activated receptor gamma (PPARγ) that has anti-inflammatory and antitumor activity at micromolar concentrations through PPARγ-dependent and/or PPARγ-independent pathways. We investigated the inhibitory activity of 15d-PGJ_2 on the bone loss that is associated with breast cancer bone metastasis and estrogen deficiency caused by cancer treatment. 15d-PGJ_2 dose-dependently inhibited viability, migration, invasion, and parathyroid hormone-related protein (PTHrP) production in MDA-MB-231 breast cancer cells. 15d-PGJ_2 suppressed receptor activator of nuclear factor kappa-B ligand (RANKL) mRNA levels and normalized osteoprotegerin (OPG) mRNA levels in hFOB1.19 osteoblastic cells treated with culture medium from MDA-MB-231 cells or PTHrP, which decreased the RANKL/OPG ratio. 15d-PGJ_2 blocked RANKL-induced osteoclastogenesis and inhibited the formation of resorption pits by decreasing the activities of cathepsin K and matrix metalloproteinases, which are secreted by mature osteoclasts. 15d-PGJ_2 exerted its effects on breast cancer and bone cells via PPARγ-independent pathways. In Balb/c *nu/nu* mice that received an intracardiac injection of MDA-MB-231 cells, subcutaneously injected 15d-PGJ_2 substantially decreased metastatic progression, cancer cell-mediated bone destruction in femora, tibiae, and mandibles, and serum PTHrP levels. 15d-PGJ_2 prevented the destruction of femoral trabecular structures in estrogen-deprived ICR mice as measured by bone morphometric parameters and serum biochemical data. Therefore, 15d-PGJ_2 may be beneficial for the prevention and treatment of breast cancer-associated bone diseases.

Introduction

Breast cancer is inextricably linked to two bone diseases, bone metastasis and osteoporosis. Metastatic breast cancer cells in the bone microenvironment disturb the balance between osteoclasts and osteoblasts, which disrupts the bone remodeling cycle and results in bone destruction [1]. Therefore, a "vicious cycle" between tumor cells and the bone microenvironment plays a critical role in breast cancer-mediated bone loss [2–3]. Four essential contributors to this vicious cycle are tumor cells, osteoblasts, osteoclasts, and resorbed bone matrix. Tumor cells produce osteolytic factors, including parathyroid hormone-related protein (PTHrP) and several interleukins [4]. These factors stimulate the expression of receptor activator of nuclear factor-kappaB (RANK) ligand (RANKL) and inhibit the production of osteoprotegerin (OPG), which is a decoy receptor of RANKL, in osteoblastic/stromal cells. RANKL triggers osteoclast differentiation via binding to RANK on osteoclast precursors [5]. Bone resorption by mature osteoclasts releases calcium and growth factors, such as transforming growth factor-beta (TGF-β) and insulin-like growth factor-1, from the bone matrix. These growth factors further stimulate tumor growth and the secretion ofosteolytic factors from tumor cells, which causes severe osteolytic lesions [3,6]. In addition to the direct harm of bone metastasis, cancer therapy for early stage and/or estrogen receptor-positive breast cancer, including cytotoxic chemotherapy, induces premature ovarian failure and hormone deprivation therapy, which ultimately increases the risk of bone loss because of estrogen deficiency [7]. Therefore, the maintenance and restoration of bone health is particularly important to promote the efficacy of cancer treatment and the quality of life in breast cancer patients.

15-deoxy-$\Delta^{12,14}$-prostaglandin J_2 (15d-PGJ$_2$) is one of the terminal products of the cyclooxygenase-mediated arachidonic acid pathway, and it is an endogenous ligand of peroxisome proliferator-activated receptor gamma (PPARγ) [8]. Its cyclopentenone structure forms a covalent adduct with cysteine residues in protein targets, which contributes to its anti-inflammatory activity at micromolar concentrations [9]. Unlike pro-inflammatory prostaglandins, 15d-PGJ$_2$ suppresses proliferation and induces apoptosis in different cancer cells [10–16]. 15d-PGJ$_2$ inhibited the invasive capacities of MDA-MB-231 human breast cancer cells via by upregulating a tissue inhibitor of matrix metalloproteinase-1 and decreasing gelatinase activity in conditioned media [17]. However, 15d-PGJ$_2$ increased the expression of matrix metalloproteinase (MMP)-1 and vascular endothelial growth factor to induce angiogenesis in MCF-7 breast cancer cells [18,19]. PPARγ activation by rosiglitazone induced bone loss by reducing osteoblast differentiation and activating osteoclast differentiation [20]. However, a recent study showed that rosiglitazone inhibited TNF-α-induced osteoclast differentiation and bone resorption [21]. Several studies also demonstrated the inhibitory effect of PPARγ agonists, including 15d-PGJ$_2$, ciglitazone, and troglitazone, on osteoclast formation [22–24].

This study determined the inhibitory activity of 15d-PGJ$_2$ on cancer-associated bone diseases. We examined the effect of 15d-PGJ$_2$ on the viability, migration, invasion, and secretion of PTHrP in MDA-MB-231 metastatic human breast cancer cells, RANKL and OPG expression in hFOB1.19 osteoblastic cells, RANKL-induced osteoclastogenesis in mouse bone marrow macrophages, and bone resorption by mature osteoclasts. We further evaluated the effect of 15d-PGJ$_2$ on bone loss in mice that received an intracardiac inoculation of human metastatic breast cancer cells and ovariectomized mice, which reflected estrogen deficiency.

Materials and Methods

Materials

15d-PGJ$_2$ and the PPARγ antagonist GW9662 were purchased from Cayman Chemicals (Ann Arbor, MI), dissolved in dimethyl sulfoxide (DMSO), and diluted with culture media immediately prior to use. Dulbecco's modified Eagle's medium (DMEM), minimum essential medium-alpha (α-MEM), DMEM:nutrient mixture F-12 (DMEM/F-12) without phenol red, Dulbecco's phosphate-buffered saline (PBS), Hanks' balanced salt solution (HBSS), fetal bovine serum (FBS), an antibiotic-antimycotic mixture (100 U/ml penicillin and 100 μg/ml streptomycin), 0.25% trypsin-EDTA, and Geneticin (G-418) were products of Gibco-BRL (Grand Island, NY). Recombinant mouse soluble RANKL and murine macrophage-colony stimulating factor (M-CSF) were obtained from Koma Biotech (Seoul, South Korea) and R&D Systems (Minneapolis, MN), respectively. Zoledronic acid (di-sodium salt) was purchased from Enzo Life Sciences (Farmingdale, NY) and D-luciferin potassium salt was obtained from Goldbio Technology (St. Louis, MO). Histopaque-1083, 3-(4,5-dimethylthiazol-2-yl)-2,5-diphenyltetrazolium bromide (MTT), 17β-estradiol (E2), and DMSO were obtained from Sigma-Aldrich (St. Louis, MO). All reagents used in this study were of analytical grade.

Cell culture

MDA-MB-231 human mammary carcinoma cells (Korean Cell Line Bank, Seoul, South Korea) were cultured in DMEM supplemented with 10% FBS and a 1% antibiotic-antimycotic mixture at 37°C under a humidified atmosphere of 5% CO_2. Human fetal osteoblastic hFOB1.19 cells (American Type Culture Collection, Manassas, VA) were grown in DMEM/F-12 without phenol red, containing 10% FBS, 1% antibiotic-antimycotic mixture, and 0.3 mg/ml G418 at 34°C in 5% CO_2 in a humidified incubator. Mouse bone marrow macrophages (BMMs) were isolated from the tibiae of male ICR mice using histopaque density gradient centrifugation as described previously [6] and cultured in α-MEM containing 10% FBS, 1% antibiotic-antimycotic mixture, and 30 ng/ml M-CSF at 37°C in a humidified atmosphere of 5% CO_2.

Animals

Male ICR mice (3 weeks old, 20 ± 3 g), female Balb/c *nu/nu* mice (5 weeks old, 20 ± 3 g), and female sham-operated and ovariectomized (OVX) ICR mice (8–9 weeks old, 28 ± 2 g) were obtained from Central Lab Animal (Seoul, South Korea). The mice were provided free access to a standard chow diet (Orient, Seongnam, Korea) and tap water *ad libitum* and housed under specific pathogen-free conditions with a 12-h light/dark cycle and a relative humidity of 50 ± 5% at 22 ± 2°C. The Institutional Animal Care and Use Committee of Department of Laboratory Animal Resources, Yonsei Biomedical Research Institute, Yonsei University College of Medicine approved all animal experiments.

Luciferase vector construction and transfection

The firefly luciferase gene from *Photinus pyralis* was amplified using polymerase chain reaction (PCR)-based methods and a pTAL-Luc vector (Clontech Laboratories, Palo Alto, CA) followed by subcloning into the pLenti6/V5 Directional TOPO cloning vector in the ViraPower Lentiviral Expression System (Invitrogen, Carlsbad, CA) to generate lentiviral particles with lentiviral vector-based luciferase. The pLenti6/V5-Luc plasmid was subjected to DNA sequencing analysis to confirm successful construction. Lentivirus particles were produced using cotransfection of the 293FT producer cell line with the pLenti6/V5-Luc plasmid and ViraPower Packaging Mix. Cells were transduced using 2 x 10^7 lentiviral particles in the transduction enhancer

Polybrene at 10 μg/ml to establish luciferase-transfected MDA-MB-231 stable cells (MDA-MD-231/Luc$^+$). Blasticidin (10 μg/ml) was added to select stably transduced cells. Blasticidin-resistant clones exhibited V5 epitope detection against an anti-V5 antibody on Western blot analysis and revealed the maximum level of luciferase activity in a microplate spectrofluorometer (Molecular Devices, Palo Alto, CA).

Cell viability assay

MDA-MB-231 cells (1 x 10^4 cells/well) were seeded into a 96-well plate with 10% FBS-DMEM. The cells were incubated in serum-free media with various concentrations of 15d-PGJ$_2$ for 24 or 72 h. hFOB1.19 human osteoblastic cells (1x 10^4 cells/well) were incubated in serum-free media with the indicated concentrations of 15d-PGJ$_2$ for 6 h or 24 h. BMMs (5 x 10^4 cells/well) were cultured in media with the indicated concentrations of 15d-PGJ$_2$ in the presence of 10% FBS and 30 ng/ml M-CSF for 5 days. Cell viability was determined using the MTT assay as described previously [6].

Cell migration assay

MDA-MB-231 cells were seeded in a 6-well plate and allowed to grow to 90% confluency. One artificial wound per well was scratched into monolayers using the narrow end of a sterile micropipette tip, and the wounded areas were photographed. Cells were incubated in serum-free DMEM with mitomycin (5 μg/ml) and various concentrations of 15d-PGJ$_2$. The scratched areas were photographed again 40 h later at the identical location of the initial image. The width of the wounded cell monolayer was measured using ImageJ software, and the percentage of wound closure was derived using the following formula: (1–(current wound width/initial wound width)) × 100.

Transwell invasion assay

A cell invasion assay was performed using a Transwell chamber (Corning, Cambridge, MA) that contained a polycarbonate membrane filter (6.5 mm diameter, 8 μm pore size). The bottom of the filter was coated with 0.1% (w/v) gelatin. Matrigel (BD Biosciences, San Jose, CA), which is a mixture of basement membrane extracellular matrix proteins, was diluted with DMEM to a final concentration of 1 mg/ml and applied to coat the membrane filter. MDA-MB-231 cell suspensions (2 x 10^4 cells/100 μl) with various concentrations of 15d-PGJ$_2$ were added to the inserts of each coated Transwell. The lower chamber contained 600 μl of media with 1% FBS and 15d-PGJ$_2$. Transwell chambers were incubated for 24 h at 37°C. Cells were fixed with 70% methanol, and the membranes were stained with hematoxylin. Non-invading cells on the upper surface of the membrane were scraped with cotton swabs, and invading cells that remained on the bottom surface were mounted on slides. Four random fields for each membrane were captured, and cells in the captured fields were quantified under a Zeiss AXio imager microscope (Carl Zeiss AG, Göttingen, Germany).

PTHrP assay

MDA-MB-231 cells were seeded at a density of 1 x 10^5 cells into a 96-well plate and incubated to adhere overnight. Cells were treated with the indicated concentrations of 15d-PGJ$_2$, TGF-β, and/or GW9662 for 24 h. The plate was centrifuged, and media were collected. PTHrP levels in the collected culture media were quantified using a human PTHrP enzyme-linked immunosorbent assay (ELISA) kit (USCN Life Science, Wuhan, China) [25].

Western blot analysis

MDA-MB-231 cells were seeded at 1 x 10^6 cells in 100 mm cell culture dishes and incubated with the indicated concentrations of TGF-β, 15d-PGJ$_2$, and/or GW9662 for 24 h. Cells were lysed in RIPA buffer (Cell Signaling Technology, Danvers, MA) containing 1 mM phenylmethylsulfonyl fluoride and protease inhibitor cocktail tablets (Roche Diagnostics) or the nuclear/cytosol fractionation kit (BioVision, Mountain View, CA). Samples were centrifuged, and proteins in the supernatants were quantitated using BCA protein assay reagents (Pierce Biotechnology, Rockford, IL). Proteins were separated using 12% sodium dodecyl sulfate-polyacrylamide gel electrophoresis and transferred to polyvinylidene difluoride membranes (Millipore, Danvers, MA). Membranes were blocked for 1 h in 5% skim milk and incubated with rabbit anti-Smad2, rabbit anti-phosphorylated Smad2 (Cell Signaling Technology), rabbit anti-β -actin (Sigma-Aldrich), and mouse anti-Lamin B (Invitrogen) at 4°C overnight, followed by incubation with horseradish peroxidase-conjugated secondary antibody for 1 h at room temperature. Proteins were visualized using an enhanced chemiluminescence kit (GE Healthcare, Buckinghamshire, UK).

Quantitative real-time PCR

The medium was replaced with serum-free DMEM/F-12 when seeded MDA-MB-231 cells reached 70–80% confluency in 10% FBS-DMEM. Conditioned media (CM), including MDA-MB-231 cell-secreted osteolytic factors, were collected after a 24-h incubation. Osteoblastic hFOB1.19 cells (1 x 10^6 cells/100 mm culture dish) were treated with the indicated concentrations of 15d-PGJ$_2$ and/or GW9662 in DMEM with 75% CM or PTHrP (100 nM) for 6 h. Total RNA was isolated using an RNeasy Mini Kit (Qiagen, Valencia, CA). First-strand cDNA from 1 μg total RNA was synthesized using the PrimeScript RT reagent kit (TaKaRa, Dalian, China). Real-time quantitative RT-PCR was performed using the 7300 Real-Time PCR System (Applied Biosystems, Foster City, CA) and the SYBR Premix Ex Taq (TaKaRa) in a 96-well optical reaction plate according to the manufacturer's instructions. The following PCR conditions were used: initial denaturation at 95°C for 30 s, followed by 40 cycles of denaturation at 95°C for 5 s and annealing at 60°C for 31 s. Cycle threshold (Ct) values were established. Relative gene expressions of RANKL and OPG to the reference gene GAPDH were determined using the $2^{-\Delta\Delta Ct}$ method. The following primer sequences were used: RANKL, forward 5'-ATGGTG GATGGCTCATGGTTAG-3' and reverse 5'-GAGCAAAAGGCTGAGCTTCAAG-3'; OPG, forward 5′-CCAGTGACCAGATCCTGAAGCT-3′ and reverse 5′-GGTGTCTTGGT CGCCATTTT-3′; and GAPDH, forward 5′-AGTCCTTCCACGATACCAAAGT-3′ and reverse 5′-CATGAGAAGTATGACAACAGCCT-3′.

Osteoclast formation assay

BMMs (5 x 10^4 cells/well) were seeded into a 96-well plate and cultured in α-MEM with 10% FBS, 30 ng/ml M-CSF and the indicated concentrations of 15d-PGJ$_2$ in the absence or presence of 100 ng/ml RANKL. Cells were cultured for 5 days, and fresh media containing the appropriate chemicals was replaced every other day. Cells were fixed using 3.7% (v/v) formaldehyde and stained for tartrate-resistant acid phosphatase (TRAP) activity for 10 min at 37°C using the Acid Phosphatase Leukocyte kit (Sigma-Aldrich) as described previously [6,26]. TRAP-positive multinucleated cells (MNCs) with more than three nuclei were quantified as differentiated osteoclasts using an Olympus IX70 inverted microscope (Olympus Optical, Tokyo, Japan) (100x magnification).

Pit formation assay

BMMs (5 x 10^4 cells/well) were plated onto BD BioCoat Osteologic MultiTest Slides with mineralized calcium phosphate thin films (BD Biosciences) and cultured in α-MEM containing 10% FBS, 30 ng/ml M-CSF, and 100 ng/ml RANKL for 4 days as described previously [26]. Differentiated osteoclasts were treated with 15d-PGJ$_2$ at the indicated concentrations for an additional 10 days. Media were replaced every other day. Media were collected to measure cathepsin K and MMP activity, and cells were treated with 4% sodium hypochlorite. Slides were washed twice using distilled water, and resorbed pits were observed under a light microscope (100x magnification).

Cathepsin K activity assay and gelatin zymography

The activity of cathepsin K and MMPs in the collected media was measured using a SensiZyme Cathepsin K Activity Assay Kit (Sigma-Aldrich) and gelatin zymography as described previously [26]. Cathepsin K activity was calculated using a standard curve and the gelatinolytic activities of MMPs were detected as clear bands against a dark blue background.

Animal model of breast cancer bone metastasis

MDA-MB-231/Luc$^+$ cells (1 x 10^6 cells/0.1 ml in HBSS) were injected into the left cardiac ventricle of female Balb/c *nu/nu* mice as previously described [27,28]. Animals were divided into four groups of 10 mice on the following day and subcutaneously administered vehicle (PBS containing 2% DMSO) alone, 0.5 or 2 mg/kg 15d-PGJ$_2$, or 0.1 mg/kg zoledronic acid as a positive control, three times per week for six weeks. Metastatic progression in nude mice was visualized using bioluminescence imaging three and five weeks after intracardiac injections. Mice were anesthetized for imaging using a Xenogen XGI-8 Gas Anesthesia System and injected intraperitoneally with 150 mg/kg of D-luciferin potassium salt in PBS. The luciferase activity was visualized using an intensified CCD video camera connected to the *in vivo* IVIS Imaging System 200 Series (Caliper Life Sciences, Hopkinton, MA). Bioluminescence from mice was expressed as total photon flux measured in photons/sec/cm^2 per steradian (sr) using Xenogen Living Image software. Blood was collected by intracardiac puncture at the end of the experiment for the serum PTHrP assay. The femora, tibiae, and mandibles of nude mice were also collected for μCT analysis.

A murine model of ovariectomy-induced bone loss

OVX mice were divided into four groups of 10 mice, and subcutaneously administered vehicle (PBS containing 2% DMSO), 0.5 or 2 mg/kg 15d-PGJ$_2$, or 10 μg/kg E2 as a positive control, three times per week for 10 weeks. Sham-operated mice were treated with vehicle alone. Body weights were measured weekly using an electronic scale. Blood samples were collected by cardiac puncture at the end of the experimental period, and the femora were dissected.

μCT analysis

The femora, tibiae, and mandibles of nude mice and the femora of sham-operated and OVX mice were examined using a SkyScan 1076 μCT scanner (SkyScan, Aartselaar, Belgium) with 100 kV, 140 μA current, rotation step 0.6°, and camera pixel size of 35 μm as described previously [6,26]. Three-dimensional (3D) images were reconstructed based on the μCT images using SkyScan NRecon software and analyzed using SkyScan's computed tomography analyzer software (CTAn). The following parameters were analyzed in the proximal tibiae of nude mice and the distal femora of sham-operated and OVX mice for quantitative analyses of bone

histomorphometry: percent bone volume (BV/TV, %), trabecular thickness (Tb.Th, mm), trabecular number (Tb.N, mm^{-1}), trabecular separation (Tb.Sp, mm), and structure model index (SMI). Values for bone mineral density (BMD) were measured in the femora of sham-operated and OVX mice.

Determination of biochemical bone parameters

The collected blood samples were allowed to clot for 2 h at room temperature and centrifuged at 2,000 ×*g* for 20 min to obtain sera as described previously [6,26]. Serum PTHrP levels from 10 nude mice were quantified in triplicate using a specific PTHrP ELISA kit. Calcium and alkaline phosphatase (ALP) levels in the sera of sham-operated and OVX mice were determined using QuantiChrome calcium and ALP assay kits (BioAssay Systems, Hayward, CA), respectively. TRAP and C-terminal telopeptides of type I collagen (CTX) levels were measured using mouse TRAP and RatLaps enzyme immunoassay (EIA) kits (Immunodiagnostic Systems, Fountain Hills, AZ), respectively. Serum levels of osteocalcin were detected using a mouse osteocalcin EIA kit (Biomedical Technologies, Stoughton, MA), and tumor necrosis factor-alpha (TNF-α) and interleukin-1 beta (IL-1β) levels were quantified using respective commercially available ELISA kits (R&D Systems). The serum levels of these factors in 10 sham-operated and OVX mice were measured in duplicate.

Goldner's trichrome staining

Mouse femora were fixed in a 10% buffered formalin solution for 48 h, decalcified with a 10% EDTA solution, and embedded in paraffin. Five-μm–thick serial sagittal sections were stained using Goldner's trichrome according to the protocol specified by Electron Microscopy Sciences (Hatfield, PA).

Statistical analysis

Data are expressed as the means ± standard error (SEM) and analyzed using one-way ANOVA and Student's *t*-test. A value of $P < 0.05$ was considered statistically significant.

Results

15d-PGJ$_2$ reduced the viability, migration, and invasion of MDA-MB-231 breast cancer cells

The viability of MDA-MB-231 cells treated with the indicated concentrations of 15d-PGJ$_2$ for 24 or 72 h was reduced in a dose-dependent manner (Fig 1A). Cells exposed to 3, 5, 10, and 30 μM concentrations of 15d-PGJ$_2$ were viable to 91%, 65%, 54%, and 38%, respectively, after 24 h of treatment and 65%, 33%, 22%, and 8%, respectively, after 72 h of treatment. The scratch wound healing assay showed that a 40 h treatment with 15d-PGJ$_2$ at noncytotoxic concentrations inhibited the migratory ability of MDA-MB-231 cells by 32% at 0.5 μM, 46% at 1 μM, and 62% at 3 μM (Fig 1B). 15d-PGJ$_2$ also decreased cell invasion in a dose-dependent manner. The number of invaded cells was inhibited by 25%, 53%, and 73% following treatment for 24 h with 15d-PGJ$_2$ at concentrations of 0.5, 1, and 3 μM, respectively (Fig 1C).

15d-PGJ$_2$ inhibited PTHrP production in MDA-MB-231 breast cancer cells

We investigated the effect of 15d-PGJ$_2$ on the secretion of PTHrP, which plays a central role in the osteolytic bone metastasis of MDA-MB-231 cells [29]. PTHrP levels were decreased by

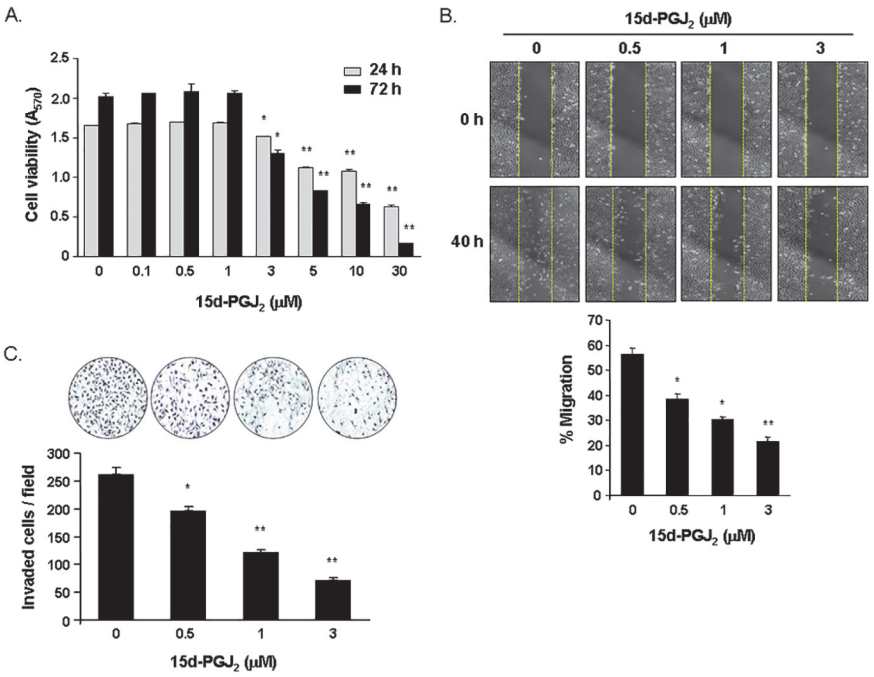

Fig 1. Effect of 15d-PGJ$_2$ on the viability, migration, and invasion of MDA-MB-231 cells. (A) Cells were incubated in serum-free media containing various concentrations of 15d-PGJ$_2$ for 24 or 72 h. Cell viability was determined using the MTT assay. (B) Cells were grown to confluency in monolayers, scratched using a micropipette tip, and treated with the indicated concentrations of 15d-PGJ$_2$ for 40 h. Scratched areas on cultured MDA-MB-231 cells were observed under a light microscope immediately and 40 h after scratching (40x magnification). Relative migrating distances of cells into scratched areas were measured using ImageJ software. Data are expressed as percentages of cell migrating distances at 40 h compared with 0 h. (C) Cells were stimulated with a 1% FBS attractant and treated with 15d-PGJ$_2$ at the indicated concentrations for 24 h. Cells that traversed across the Matrigel matrix were stained with hematoxylin, and representative images were visualized using light microscopy (200x magnification). The numbers of invaded cells were counted in four random fields per membrane filter. Data are expressed as means ± SEM. *$P<0.05$, **$P<0.001$ vs. untreated cells.

doi:10.1371/journal.pone.0122764.g001

24% in the culture media of MDA-MB-231 cells treated with 1 μM 15d-PGJ$_2$ for 24 h and 39% with 3 μM 15d-PGJ$_2$ (Fig 2A). TGF-β stimulation elevated PTHrP levels in the culture media by 1.6-fold, but treatment with 3 μM 15d-PGJ$_2$ noticeably inhibited TGF-β-induced PTHrP production in MDA-MB-231 cells. Treatment with GW9662, a PPAR-γ antagonist, did not normalize the reduced PTHrP levels following 15d-PGJ$_2$ treatment in MDA-MB-231 cells regardless of TGF-β treatment (Fig 2B). 15d-PGJ$_2$ treatment inhibited the substantial enhancement in Smad2 phosphorylation and nuclear levels of pSmad2 in TGF-β -stimulated cells. The inhibitory effect of 15d-PGJ$_2$ on TGF-β -induced activation of Smad2 remained in the presence of GW9662 (Fig 2C). These results demonstrate that 15d-PGJ$_2$ inhibits PTHrP production through a PPARγ-independent pathway in MDA-MB-231 breast cancer cells regardless of TGF- stimulation.

15d-PGJ$_2$ inhibited the RANKL/OPG ratio in hFOB1.19 osteoblastic cells

15d-PGJ$_2$ treatment at concentrations less than 5 μM for 6 h did not show cytotoxic effects, but a 24-h treatment inhibited cell viability by 47% at 3 μM and 60% at 10 μM in hFOB1.19 human osteoblastic cells (Fig 3A). Real-time PCR analysis indicated that RANKL mRNA levels increased considerably and OPG mRNA levels decreased noticeably in osteoblastic hFOB1.19

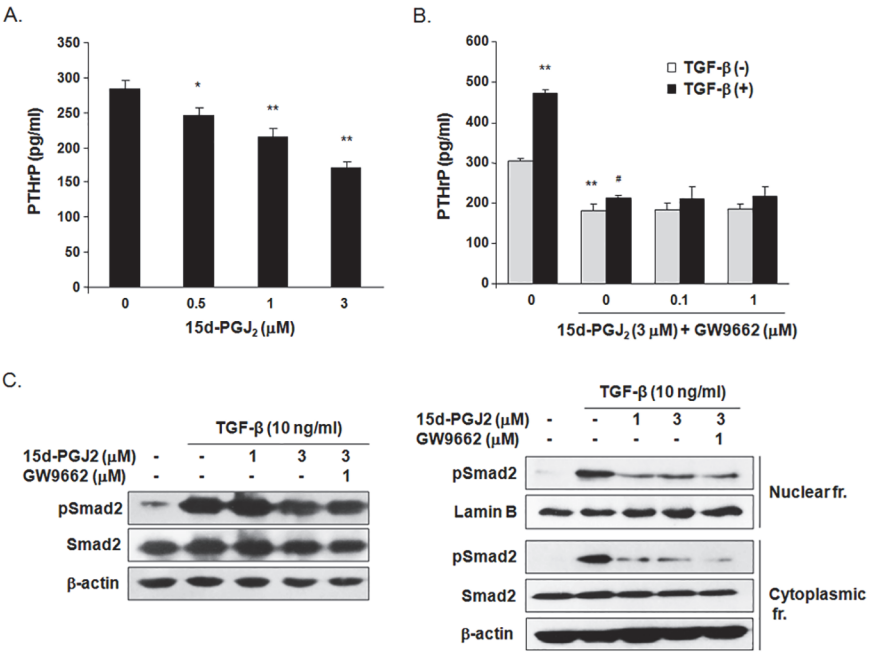

Fig 2. Effect of 15d-PGJ$_2$ on PTHrP production in MDA-MB-231 cells. The cells were treated with (A) various concentrations of 15d-PGJ$_2$ or (B) TGF-β, 15d-PGJ$_2$ and/or GW9662 for 24 h. PTHrP levels were measured in the cultured media of MDA-MB-231 cells using a commercial human PTHrP ELISA kit. Data are expressed as the means ± SEM. *P<0.05, **P<0.01 vs. untreated cells. $^{\#}P$<0.01 vs. TGF-β -treated cells. (C) The level of Smad2 in total lysates and nuclear and cytoplasmic fractions was determined using western blotting in MDA-MB-231 cells stimulated by TGF- β, 15d-PGJ$_2$ and/or GW9662 PPARγ antagonist for 24 h. The cropped blots are representative of experiments that were repeated three times.

doi:10.1371/journal.pone.0122764.g002

cells stimulated with 75% CM from MDA-MB-231 breast cancer cells or PTHrP (100 nM) for 6 h, which elevated the RANKL/OPG ratio. However, treatment with 15d-PGJ$_2$ dose-dependently suppressed the CM- and PTHrP-induced increase in the RANKL/OPG ratio by blocking increases in RANKL mRNA levels and decreases in OPG mRNA levels in hFOB1.19 cells exposed to CM and PTHrP, respectively (Fig 3B). GW9662 treatment did not rescue RANKL and OPG mRNA levels that were altered by 15d-PGJ$_2$ treatment in CM and PTHrP-treated hFOB1.19 cells. These results indicate that 15d-PGJ$_2$ inhibits the RANKL/OPG ratio in hFOB1.19 cells stimulated with MDA-MB-231 cell-derived osteolytic factors, particularly PTHrP.

15d-PGJ$_2$ inhibited RANKL-induced osteoclast differentiation and activity

Treatment with 15d-PGJ$_2$ for 5 days inhibited cell viability by 19% at a concentration of 3 μM, 36% at 5 μM, and 53% at 10 μM in BMMs. BMMs were differentiated to TRAP-positive multinucleated cells as osteoclasts in the presence of M-CSF and RANKL for 5 days, but treatment with 15d-PGJ$_2$ inhibited RANKL-induced osteoclast formation in a dose-related manner. Treatment with 0.5, 1, and 3 μM 15d-PGJ$_2$ reduced the number of differentiated osteoclasts by 32%, 55%, and 93%, respectively. GW9662 treatment did not attenuate the inhibitory effect of 15d-PGJ$_2$ on RANKL-induced osteoclast formation (Fig 4A). The formation of resorption pits determined the activity of mature osteoclasts. Osteoclast differentiation was induced on calcium phosphate-coated plates, and cells were incubated with 15d-PGJ$_2$ in the presence of M-CSF and RANKL for 10 days. Treatment with 15d-PGJ$_2$ dose-dependently suppressed the

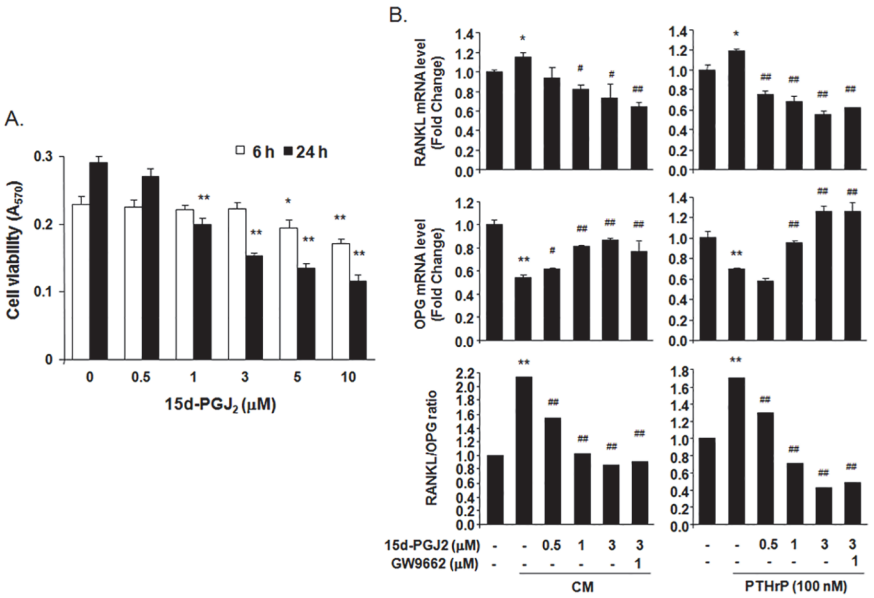

Fig 3. Effect of 15d-PGJ$_2$ on RANKL and OPG mRNA expression in hFOB1.19 human osteoblastic cells. (A) hFOB1.19 cells were treated with the indicated concentrations of 15d-PGJ$_2$ in DMEM/F12 for 6 h or 24 h. Cell viability was determined using the MTT assay. (B) hFOB1.19 cells were treated with the indicated concentrations of 15d-PGJ$_2$ in DMEM/F12 containing 75% CM of MDA-MB-231 cells or PTHrP (100 ng) for 6 h. mRNA levels of RANKL and OPG were analyzed using real time-PCR. Graphs are expressed as the ratio of the densitometric intensity of RANKL to OPG after normalization to GAPDH. Data represent the means ± SEM. $^{*}P<0.05$, $^{**}P<0.001$ vs. untreated cells, $^{\#}P<0.05$, $^{\#\#}P<0.001$ vs. CM- or PTHrP-treated cells.

doi:10.1371/journal.pone.0122764.g003

formation of resorbed areas (Fig 4B). RANKL treatment significantly increased the activity of cathepsin K in cultured media, but 15d-PGJ$_2$ treatment suppressed the activity almost to control levels (Fig 4C). Gelatin zymography indicated that the levels of pro- and active forms of MMP-2 and MMP-9 were considerably enhanced in cultured media of RANKL-induced mature osteoclasts, but 15d-PGJ$_2$ treatment decreased the levels of these MMPs in a dose-dependent manner (Fig 4D).

15d-PGJ$_2$ inhibited osteolytic bone metastasis by breast cancer cells in nude mice

MDA-MB-231/Luc$^+$ cells were inoculated into the left ventricles of nude mice to induce bone metastasis of breast cancer cells, and 15d-PGJ$_2$ or zoledronic acid was subcutaneously injected for six weeks. Bioluminescence imaging showed that subcutaneous administration of 15d-PGJ$_2$ or zoledronic acid for three and five weeks inhibited the metastatic progression of MDA-MB-231/Luc$^+$ cells (Fig 5A). Osteolytic lesions of all mice were analyzed using μCT six weeks after cancer cell injections. Radiographic images of MDA-MB-231/Luc$^+$ cell-injected mice indicated that osteolytic lesions were substantially developed in mandibles, distal femora, and proximal tibiae. However, 15d-PGJ$_2$ or zoledronic acid administration inhibited cancer cell-induced osteolytic lesions in a dose-dependent manner (Fig 5B). 3D-images also revealed that MDA-MB-231/Luc$^+$ cells induced severe destruction in the inner part of the mandible, but treatment with 15d-PGJ$_2$ or zoledronic acid noticeably reduced this damage (Fig 5C). Bone morphometric analyses demonstrated that the injection of MDA-MB-231/Luc$^+$ cells decreased BV/TV, Tb.Th, and Tb.N and increased Tb.Sp and SMI, but treatment with 15d-PGJ$_2$ or zoledronic acid induced a recovery of these bone morphometric parameters. Furthermore, the

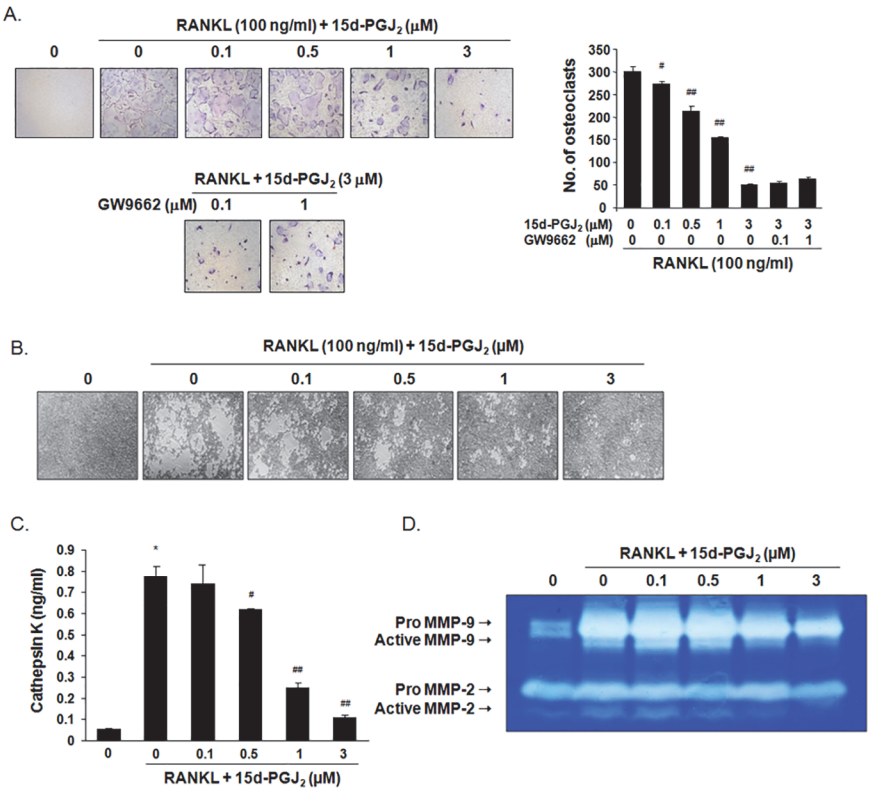

Fig 4. Effect of 15d-PGJ$_2$ on RANKL-induced osteoclast differentiation and activation. (A) BMMs isolated from ICR mice were treated with M-CSF (30 ng/ml), RANKL (100 ng/ml), 15d-PGJ$_2$, and/or GW9662 for 5 days. TRAP staining was performed to detect osteoclast formation. TRAP-positive multinucleated cells ($\geq$ 3 nuclei) as differentiated osteoclasts were observed (100x magnification) and counted under an inverted microscope. (B) The differentiated BMMs were treated with 15d-PGJ$_2$ in the presence of M-CSF (30 ng/ml) and RANKL (100 ng/ml) for an additional 10 days. The formed resorption pits were visualized using light microscopy (100x magnification). (C) The level of cathepsin K in the cultured media was measured using a commercially available ELISA kit. (D) The activities of MMPs were determined using gelatin zymograpy as clear bands against a blue background that corresponded to active MMP-2/9 (62/92 kDa) and pro-MMP-2/9 (72/105 kDa). The cropped gel image is representative of experiments that were repeated three times. Data are expressed as the means ± SEM. *P<0.001 vs. RANKL-untreated cells. $^{\#}P$<0.05, $^{\#\#}P$<0.001 vs. RANKL-treated cells.

doi:10.1371/journal.pone.0122764.g004

levels of PTHrP were significantly increased in the sera of mice that received an intracardiac injection of MDA-MB-231/Luc$^+$ cells, but treatment with 15d-PGJ$_2$ or zoledronic acid inhibited the increase in PTHrP levels (Fig 5D).

15d-PGJ$_2$ inhibited ovariectomy-induced bone loss

Ovariectomy-induced osteoporosis is commonly used as an animal model of bone loss due to estrogen deficiency in humans [30]. μCT analysis showed that BMD, BV/TV, Tb.Th and Tb.N decreased, but Tb.Sp and SMI increased, in OVX mice compared to the sham group. However, these bone morphometric parameters significantly recovered to control levels in 15d-PGJ$_2$- or E2-treated OVX mice (Fig 6A). 3D-images and Goldner's trichrome staining of distal femoral metaphyses revealed that the subcutaneous administration of 15d-PGJ$_2$ or E2 in OVX mice dose-dependently suppressed severe trabecular bone loss in OVX mice (Fig 6B). In addition, treatment with 15d-PGJ$_2$ or E2 blocked elevations in body weight in OVX mice. We measured ALP activity and osteocalcin level as markers of bone formation and calcium, TRAP, and CTX

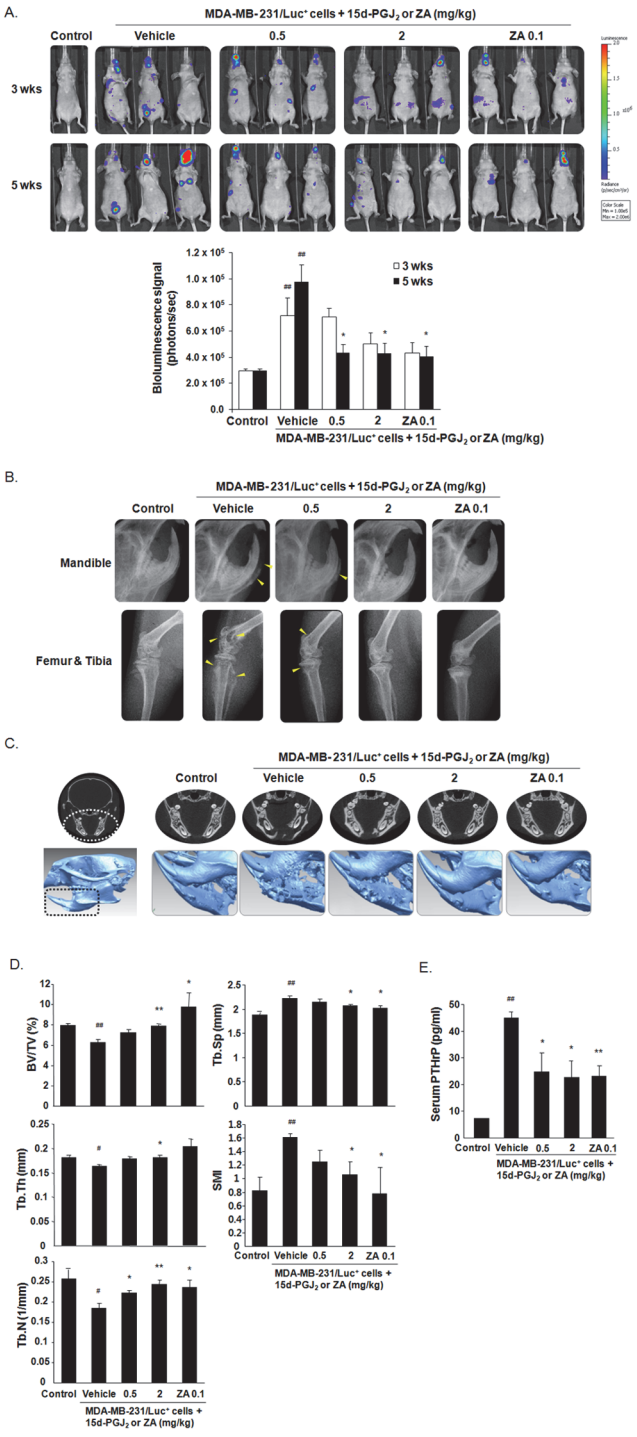

Fig 5. Effect of 15d-PGJ$_2$ on osteolytic bone metastasis in nude mice that received intracardiac injections of MDA-MB-231 cells. MDA-MB-231/Luc$^+$ cells were inoculated into the left ventricles of female nude mice. 15d-PGJ$_2$ or zoledronic acid (ZA) was subcutaneously injected 3 times per week for 6 weeks at the indicated doses (n = 10). (A) Metastatic progression was detected by measuring bioluminescence in the same mice at 3 and 5 weeks after the injection of cancer cells. The formed metastases were quantified by measuring total photon flux per second. (B) Radiographic images of mandibles, distal femora, and proximal tibiae were scanned using μCT 6 weeks after the injection of cancer cells. Arrowheads indicate osteolytic lesions. (C) The mandibles of mice were analyzed using 3D-images. (D) Bone morphometric parameters, including BV/TV, Tb.N, Tb.Th, Tb.Sp, and SMI, were measured using μCT analysis of the proximal tibiae from mice. (E) Serum PTHrP levels were assayed using a commercially available ELISA kit. Data are

expressed as the means ± SEM. $^{\#}P<0.05$, $^{\#\#}P<0.01$ vs. control group.*$P<0.05$, **$P<0.01$ vs. vehicle-treated group inoculated with cancer cells.

doi:10.1371/journal.pone.0122764.g005

were used as the markers of bone resorption. The serum levels of these bone turnover markers were elevated significantly in OVX mice, but these levels noticeably decreased in 15d-PGJ$_2$- or E2-treated OVX mice (Fig 6C). Treatment with 15d-PGJ$_2$ or E2 also significantly reduced TNF-α and IL-1β levels in the sera of OVX mice (Fig 6D).

Discussion

The present study determined the inhibitory activity of 15d-PGJ$_2$ on breast cancer-associated bone diseases. We first investigated whether 15d-PGJ$_2$ blocked breast cancer bone metastasis and the resulting bone loss. We found that 15d-PGJ$_2$ attenuated cell migration and the invasion of MDA-MB-231 human breast cancer cells at noncytotoxic concentrations. Treatment with 15d-PGJ$_2$ reduced the secreted levels of PTHrP through a PPARγ-independent pathway in MDA-MB-231 cells regardless of TGF-β stimulation. Cancer cell-derived PTHrP attracted attention as a key mediator of the triggering and intensification of the vicious cycle of osteolytic bone metastasis in the bone microenvironment [31]. Among the bone matrix-derived growth factors, TGF-β regulates PTHrP production via Smad-dependent or Smad-independent pathways [32–34]. Our data indicated that 15d-PGJ$_2$ inhibited Smad2 phosphorylation regardless of the PPARγ pathway, and consequently, reduced levels of pSmad2 were detected in the nucleus and cytoplasm. These results suggest that treatment with 15d-PGJ$_2$ suppresses the metastatic progression of MDA-MB-231 cells and decreases PTHrP production through a PPAR-independent but Smad2-dependent pathway in MDA-MB-231 cells that primarily metastasized into bone.

The majority of patients with breast cancer bone metastasis exhibit osteolytic lesions that are accompanied by severe bone destruction. Osteolysis is caused by mature osteoclasts derived from hematopoietic mononuclear precursors not a direct effect of cancer cells on bone [35]. Almost all of the other mediators that induce osteoclast differentiation and activation transduce and amplify signals through RANKL, which is produced by osteoblastic stromal cells [5]. PTHrP also enhances osteoclastogenesis and the activity of mature osteoclasts via an up-regulation of RANKL and down-regulation of its decoy receptor OPG in osteoblasts [36]. Noncytotoxic concentrations of 15d-PGJ$_2$ significantly inhibited an increase in RANKL mRNA expression and a decrease in OPG mRNA expression in hFOB1.19 human osteoblastic cells stimulated with an MDA-MB-231 cell-derived conditioned medium or PTHrP in our study. Osteoclasts that are differentiated by RANKL produce acidic conditions to dissolve calcium hydroxyapatite and secrete various proteolytic enzymes, such as cathepsin K and MMPs, to degrade organic components in the bone matrix, which releases bone-stored growth factors [37,38]. Therefore, the inhibition of osteoclast-mediated bone resorption can ultimately contribute to the prevention of additional tumor growth and cancer cell-mediated osteolysis. 15d-PGJ$_2$ reduced RANKL-induced osteoclast differentiation and inhibited the formation of osteoclast-mediated resorption pits by suppressing the proteolytic activities of cathepsin K and MMP-2/9. Treatment with GW9662 did not affect the anti-osteoclastogenic activity of 15d-PGJ$_2$. These results indicate that 15d-PGJ$_2$ blocks breast cancer-mediated bone destruction by reducing the RANKL/OPG ratio in osteoblasts that are exposed to MDA-MB-231 cell-derived osteolytic factors and inhibiting the formation and function of osteoclasts in RANKL-treated osteoclast precursors in a PPAR-independent manner.

We further estimated the inhibitory activity of 15d-PGJ$_2$ on osteolytic bone metastasis in nude mice inoculated with MDA-MB-231/Luc$^+$ cells into the left cardiac ventricle and

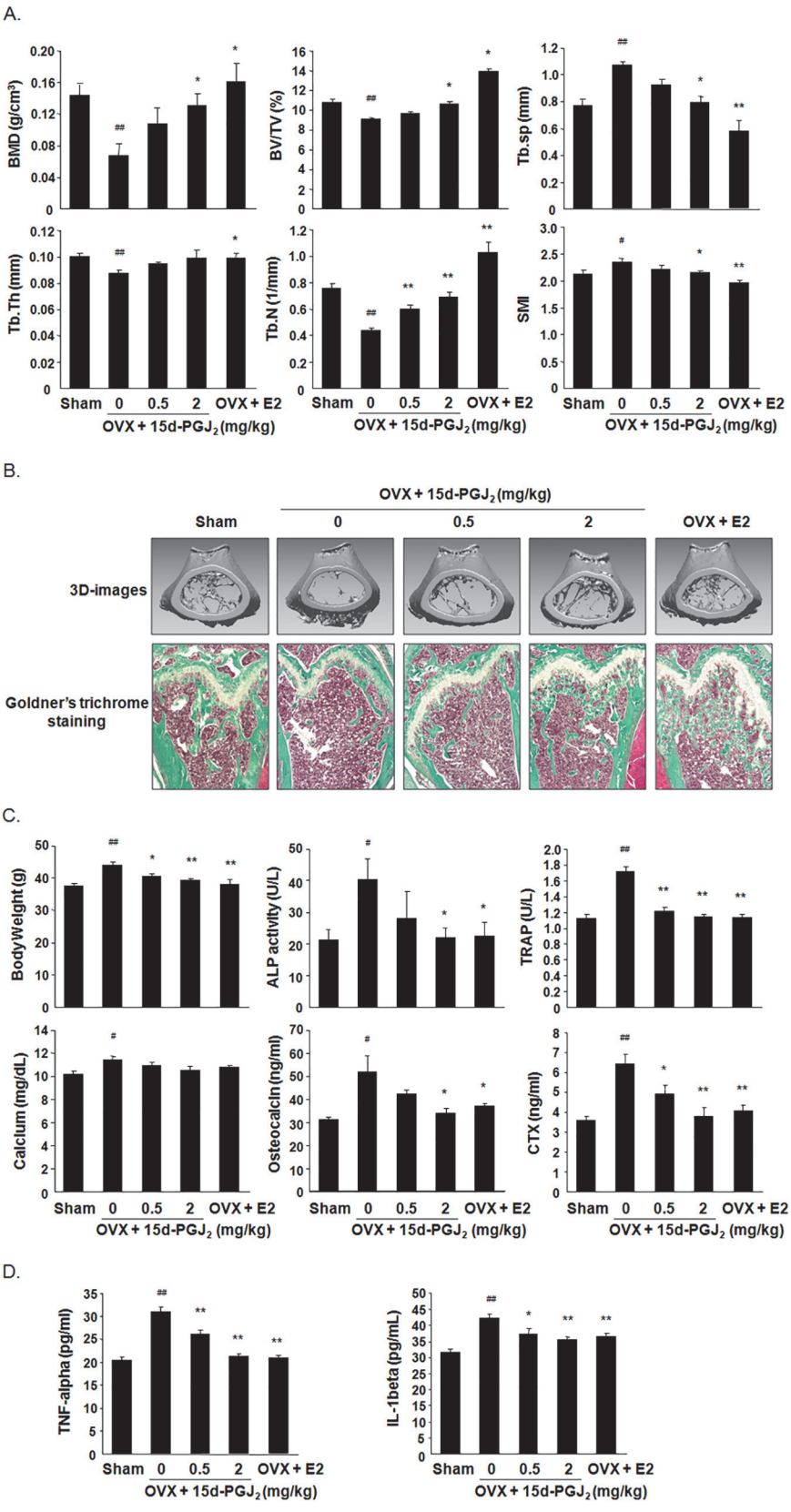
A.
BMD (g/cm³)
BV/TV (%)
Tb.sp (mm)
Tb.Th (mm)
Tb.N (1/mm)
SMI
Sham 0 0.5 2 OVX + E2
OVX + 15d-PGJ2 (mg/kg)
B.
OVX + 15d-PGJ2 (mg/kg)
Sham
0
0.5
2
OVX + E2
3D-images
Goldner's trichrome staining
C.
BodyWeight (g)
ALP activity (U/L)
TRAP (U/L)
Calcium (mg/dL)
Osteocalcin (ng/ml)
CTX (ng/ml)
D.
TNF-alpha (pg/ml)
IL-1beta (pg/mL)

Fig 6. Effect of 15d-PGJ$_2$ on ovariectomy-induced bone loss. OVX mice were subcutaneously injected with vehicle, 15d-PGJ$_2$, or E2 (10 μg/kg) for 10 weeks (n = 10). Sham-operated mice received vehicle alone (n = 10). (A) Bone morphometric parameters, including BMD, BV/TV, Tb.Th, Tb.N, Th.Sp, and SMI, were measured using μCT analysis of the femora from mice. (B) 3D images of distal femora of mice were obtained from the reconstruction of μCT data (upper). Sagittal sections of distal femora from mice were stained with Goldner's trichrome. Bone trabeculae appear green, and bone marrow appears red. Stained sections were photographed using a light microscope (100x magnification). (C) Body weights of all mice were measured, and blood sera were collected from all mice for analyses of biochemical parameters. Serum levels of calcium, ALP, osteocalcin, TRAP, and CTX were evaluated using the respective kits as described in Materials and Methods. (D) Serum levels of TNF-α and IL-1β were determined using specific ELISA kits. Data are expressed as the means ± SEM. $^{\#}P< 0.05$, $^{\#\#}P< 0.01$ vs. sham group. $^{*}P<0.05$, $^{**}P<0.01$ vs. OVX group.

doi:10.1371/journal.pone.0122764.g006

subcutaneously injected with 15d-PGJ$_2$ or zoledronic acid for six weeks. Metastatic progression was delayed and osteolytic lesions in mandibles, femora, and tibiae were decreased in 15d-PGJ$_2$-treated mice, which was supported by bioluminescence imaging, radiographic and 3D images, and bone morphometric parameters. Moreover, the reduced serum PTHrP levels in MDA-MB-231cell-injected mice treated with15d-PGJ$_2$ may be linked with the *in vitro* inhibitory effect of 15d-PGJ$_2$ on PTHrP production. Zoledronic acid used as a positive control is an anti-bone resorptive agent administered to cancer patients with bone metastases at the clinical dose of 4 mg via intravenous injection every 3–4 weeks [39]. Although treatment with clinical doses of bisphosphonates (a daily dose 3 μg/kg or a weekly dose of 20 μg/kg) has been reported to inhibit skeletal tumor growth in murine models [39], zoledronic acid at high doses, 0.1 or 0.125 mg/kg, was administered to exhibit its *in vivo* anti-tumor effect in recent studies [40–42]. In this study, zoledronic acid at 0.1 mg/kg also reduced bone metastasis and bone loss in mandibles, femora, and tibiae in mice with intracardiac injection of MDA-MB-23l cells. 15d-PGJ$_2$ at 2 mg/kg showed a similar effect with zoledronic acid at 0.1 mg/kg. These results demonstrate that administration of 15d-PGJ$_2$ inhibits the bone metastasis of breast cancer and the resulting bone destruction.

Currently, the main clinical drugs for the treatment of cancer-associated skeletal lesions are inhibitors of osteoclastic bone resorption, including bisphosphonates and denosumab as a monoclonal antibody against RANKL [43]. These agents are beneficial for the prevention and treatment of osteoporosis in postmenopausal women [44]. In addition, bisphosphonates and denosumab decrease estrogen deficiency-related bone loss due to aromatase inhibitor therapy and cytotoxic chemotherapy in cancer patients [7]. We determined whether 15d-PGJ$_2$, which exhibits potent anti-osteoclastic and anti-bone resorptive activity, prevented bone loss in OVX mice as a standard model for the pharmaceutical evaluation of estrogen deficiency-induced osteoporosis. Subcutaneously administered 15d-PGJ$_2$ delayed weight gain and damage to femoral trabecular bone in OVX mice, as evidenced by bone morphometric parameters, reconstructed 3D images, histological analyses, and biochemical parameters. The serum levels of the pro-inflammatory cytokines TNF-α and IL-1β, which are key mediators of bone loss following estrogen withdrawal via the promotion of osteoclastic bone resorption [45], were also reduced in 15d-PGJ$_2$-treated OVX mice. These results indicate that 15d-PGJ$_2$ prevents bone loss during estrogen deficiency-inducing cancer treatment.

In summary, 15d-PGJ$_2$ inhibited the proliferation, migration, and invasion of MDA-MB-231 cells and the production of a major osteolytic factor, PTHrP. 15d-PGJ$_2$ also suppressed the RANKL/OPG ratio in osteoblastic cells exposed to breast cancer cell-derived osteolytic factors, the RANKL-induced differentiation of osteoclast precursors, and the formation of resorbed pits by decreasing the activities of cathepsin K and MMPs. Furthermore, subcutaneous injections of 15d-PGJ$_2$ reduced the metastasis of breast cancer cells into bone and the generation of osteolytic lesions in mice. Treatment with 15d-PGJ$_2$ inhibited estrogen deficiency-induced

bone loss. Therefore, 15d-PGJ$_2$ and 15d-PGJ$_2$-inducing agents may be potent candidates for the prevention and treatment of bone loss caused by breast cancer bone metastasis and chemotherapy.

Acknowledgments

The authors thank Chae-Eun Lee in the Oral Science Research Institute for technical assistance for μCT and Won-Gyeong Ahn at the Chuncheon Center of the Korea Basic Science Institute for technical assistance in real-time IVIS Imaging System 200.

Author Contributions

Conceived and designed the experiments: KKP WYC. Performed the experiments: KRK. Analyzed the data: KRK KKP HJK SKL WYC. Contributed reagents/materials/analysis tools: KRK HJK SKL GTM. Wrote the paper: KRK WYC.

References

1. Suva LJ, Washam C, Nicholas RW, Griffin RJ. Bone metastasis: mechanisms and therapeutic opportunities. Nat Rev Endocrinol. 2011; 7: 208–218. doi: 10.1038/nrendo.2010.227 PMID: 21200394
2. Coleman RE. Clinical features of metastatic bone disease and risk of skeletal morbidity. Clin Cancer Res. 2006; 12: 6243s–6249s. PMID: 17062708
3. Kozlow W, Guise TA. Breast cancer metastasis to bone: mechanisms of osteolysis and implications for therapy. J Mammary Gland Biol Neoplasia. 2005; 10: 169–180. PMID: 16025223
4. Esposito M, Kang Y. Targeting tumor-stromal interactions in bone metastasis. Pharmacol Ther. 2014; 141: 222–233. doi: 10.1016/j.pharmthera.2013.10.006 PMID: 24140083
5. Azim HA, Kamal NS, Azim HA Jr. Bone metastasis in breast cancer: the story of RANK-ligand. J Egypt Natl Canc Inst. 2012; 24: 107–114. doi: 10.1016/j.jnci.2012.06.002 PMID: 22929916
6. Lee SK, Park KK, Park JH, Lim SS, Chung WY. The inhibitory effect of roasted licorice extract on human metastatic breast cancer cell-induced bone destruction. Phytother Res. 2013; 27: 1776–1783. doi: 10.1002/ptr.4930 PMID: 23401151
7. Brufsky AM. Cancer treatment-induced bone loss: pathophysiology and clinical perspectives. Oncologist. 2008; 13: 187–195. doi: 10.1634/theoncologist.2007-0152 PMID: 18305064
8. Diez-Dacal B, Perez-Sala D. Anti-inflammatory prostanoids: focus on the interactions between electrophile signaling and resolution of inflammation. Scientific World Journal. 2010; 10: 655–675. doi: 10.1100/tsw.2010.69 PMID: 20419278
9. Surh YJ, Na HK, Park JM, Lee HN, Kim W, Yoon IS, et al. 15-deoxy-$\Delta^{12,14}$-prostaglandin J_2, an electrophilic lipid mediator of anti-inflammatory and pro-resolving signaling. Biochem Pharmacol. 2011; 82: 1335–1351. doi: 10.1016/j.bcp.2011.07.100 PMID: 21843512
10. Ishihara S, Rumi MA, Okuyama T, Kinoshita Y. Effect of prostaglandins on the regulation of tumor growth. Curr Med Chem Anticancer Agents. 2004; 4: 379–387. PMID: 15281909
11. Shen ZN, Nishida K, Doi H, Oohashi T, Hirohata S, Ozaki T, et al. Suppression of chondrosarcoma cells by 15-deoxy-Delta 12,14-prostaglandin J2 is associated with altered expression of Bax/Bcl-xL and p21. Biochem Biophys Res Commun. 2005; 328: 375–382. PMID: 15694358
12. Ciucci A, Gianferretti P, Piva R, Guyot T, Snape TJ, Roberts SM, et al. Induction of apoptosis in estrogen receptor-negative breast cancer cells by natural and synthetic cyclopentenones: role of the IkappaB kinase/nuclear factor-kappaB pathway. Mol Pharmacol. 2006; 70: 1812–1821. PMID: 16908599
13. Ray DM, Akbiyik F, Phipps RP. The peroxisome proliferator-activated receptor gamma (PPARgamma) ligands 15-deoxy-$\Delta^{12,14}$-prostaglandin J_2 and ciglitazone induce human B lymphocyte and B cell lymphoma apoptosis by PPARgamma-independent mechanisms. J Immunol. 2006; 177: 5068–5076. PMID: 17015690
14. Qiao L, Dai Y, Gu Q, Chan KW, Zou B, Ma J, et al. Down-regulation of X-linked inhibitor of apoptosis synergistically enhanced peroxisome proliferator-activated receptor gamma ligand-induced growth inhibition in colon cancer. Mol Cancer Ther. 2008; 7: 2203–2211. doi: 10.1158/1535-7163.MCT-08-0326 PMID: 18645029
15. Kaikkonen S, Paakinaho V, Sutinen P, Levonen AL, Palvimo JJ. Prostaglandin 15d-PGJ(2) inhibits androgen receptor signaling in prostate cancer cells. Mol Endocrinol. 2013; 27: 212–223. doi: 10.1210/me.2012-1313 PMID: 23192983

16. Wang JJ, Mak OT. Induction of apoptosis by 15d-PGJ$_2$ via ROS formation: an alternative pathway without PPARγ activation in non-small cell lung carcinoma A549 cells. Prostaglandins Other Lipid Mediat. 2011; 94: 104–111. doi: 10.1016/j.prostaglandins.2011.01.004 PMID: 21396480

17. Liu H, Zang C, Fenner MH, Possinger K, Elstner E. PPARgamma ligands and ATRA inhibit the invasion of human breast cancer cells in vitro. Breast Cancer Res Treat. 2003; 79: 63–74. PMID: 12779083

18. Kim EH, Na HK, Surh YJ. Upregulation of VEGF by 15-deoxy-$\Delta^{12,14}$-prostaglandin J$_2$ via heme oxygenase-1 and ERK1/2 signaling in MCF-7 cells. Ann N Y Acad Sci. 2006; 1090: 375–384. PMID: 17384282

19. Kim DH, Kim JH, Kim EH, Na HK, Cha YN, Chung JH, et al. 15-Deoxy-$\Delta^{12,14}$-prostaglandin J$_2$ upregulates the expression of heme oxygenase-1 and subsequently matrix metalloproteinase-1 in human breast cancer cells: possible roles of iron and ROS. Carcinogenesis. 2009; 30: 645–654. doi: 10.1093/carcin/bgp012 PMID: 19136476

20. Wei W, Wan Y. Thiazolidinediones on PPARγ: The roles in bone remodeling. PPAR Res. 2011; 2011: 867180. doi: 10.1155/2011/867180 PMID: 22135675

21. Yang CR, Lai CC. Thiazolidinediones inhibit TNF-α-mediated osteoclast differentiation of RAW264.7 macrophages and mouse bone marrow cells through downregulation of NFATc1. Shock. 2010; 33: 662–667. doi: 10.1097/SHK.0b013e3181cc0738 PMID: 19953004

22. Hounoki H, Sugiyama E, Mohamed SG, Shinoda K, Taki H, Abdel-Aziz HO, et al. Activation of peroxisome proliferator-activated receptor gamma inhibits TNF-alpha-mediated osteoclast differentiation in human peripheral monocytes in part via suppression of monocyte chemoattractant protein-1 expression. Bone. 2008; 42: 765–774. doi: 10.1016/j.bone.2007.11.016 PMID: 18242157

23. Okazaki R, Toriumi M, Fukumoto S, Miyamoto M, Fujita T, Tanaka K, et al. Thiazolidinediones inhibit osteoclast-like cell formation and bone resorption in vitro. Endocrinology. 1999; 140: 5060–5065. PMID: 10537132

24. Mbalaviele G, Abu-Amer Y, Meng A, Jaiswal R, Beck S, Pittenger MF, et al. Activation of peroxisome proliferator-activated receptor-γ pathway inhibits osteoclast differentiation. J Biol Chem. 2000; 275: 14388–14393. PMID: 10799521

25. Park SY, Kim HJ, Kim KR, Lee SK, Lee CK, Park KK, et al. Betulinic acid, a bioactive pentacyclic triterpenoid, inhibits skeletal-related events induced by breast cancer bone metastases and treatment. Toxicol Appl Pharmacol. 2014; 275: 152–162. doi: 10.1016/j.taap.2014.01.009 PMID: 24463094

26. Jun AY, Kim HJ, Park KK, Son KH, Lee DH, Woo MH, et al. Extract of Magnoliae Flos inhibits ovariectomy induced osteoporosis by blocking osteoclastogenesis and reducing osteoclast-mediated bone resorption. Fitoterapia. 2012; 83: 1523–1531. doi: 10.1016/j.fitote.2012.08.020 PMID: 22981503

27. Park SI, Kim SJ, McCauley LK, Gallick GE. Pre-clinical mouse models of human prostate cancer and their utility in drug discovery. Curr Protoc Pharmacol. 2010;Chapter 14: Unit 14.15.

28. Campbell JP, Merkel AR, Masood-Campbell SK, Elefteriou F, Sterling JA. Models of bone metastasis. J Vis Exp. 2012; 67: e4260. doi: 10.3791/4260 PMID: 22972196

29. Guise TA, Yin JJ, Thomas RJ, Dallas M, Cui Y, Gillespie MT. Parathyroid hormone-related protein (PTHrP)-(1–139) isoform is efficiently secreted in vitro and enhances breast cancer metastasis to bone in vivo. Bone. 2002; 30: 670–676. PMID: 11996903

30. Inada M, Matsumoto C, Miyaura C. Animal models for bone and joint disease. Ovariectomized and orchidectomized animals. Clin Calcium. 2011; 21: 164–170. doi: CliCa1102164170 PMID: 21289412

31. Pratap J, Wixted JJ, Gaur T, Zaidi SK, Dobson J, Gokul KD, et al. Runx2 transcriptional activation of Indian Hedgehog and a downstream bone metastatic pathway in breast cancer cells. Cancer Res. 2008; 68: 7795–7802. doi: 10.1158/0008-5472.CAN-08-1078 PMID: 18829534

32. Safina A, Sotomayor P, Limoge M, Morrison C, Bakin AV. TAK1-TAB2 signaling contributes to bone destruction by breast carcinoma cells. Mol Cancer Res. 2011; 9: 1042–1053. doi: 10.1158/1541-7786.MCR-10-0196 PMID: 21700681

33. Lindemann RK, Ballschmieter P, Nordheim A, Dittmer J. Transforming growth factor beta regulates parathyroid hormone-related protein expression in MDA-MB-231 breast cancer cells through a novel Smad/Ets synergism. J Biol Chem. 2001; 276: 46661–46670. PMID: 11590145

34. Kakonen SM, Selander KS, Chirgwin JM, Yin JJ, Burns S, Rankin WA, et al. Transforming growth factor-beta stimulates parathyroid hormone-related protein and osteolytic metastases via Smad and mitogen-activated protein kinase signaling pathways. J Biol Chem. 2002; 277: 24571–24578. PMID: 11964407

35. Mundy GR. Metastasis to bone: Causes, consequences and therapeutic opportunities. Nat Rev Cancer. 2002; 2: 584–593. PMID: 12154351

36. Karaplis AC, Goltzman D. PTH and PTHrP effects on the skeleton. Rev Endocr Metab Disord. 2000; 1: 331–341. PMID: 11706747

37. Andersen TL, del Carmen Ovejero M, Kirkegaard T, Lenhard T, Foged NT, Delaissé JM. A scrutiny of matrix metalloproteinases in osteoclasts: evidence for heterogeneity and for the presence of MMPs synthesized by other cells. Bone. 2004; 35: 1107–1119. PMID: 15542036

38. Costa AG, Cusano NE, Silva BC, Cremers S, Bilezikian JP. Cathepsin K: its skeletal actions and role as a therapeutic target in osteoporosis. Nat Rev Rheumatol. 2011; 7: 447–456. doi: 10.1038/nrrheum.2011.77 PMID: 21670768

39. Daubiné F, Le Gall C, Gasser J, Green J, Clézardin P. Antitumor effects of clinical dosing regimens of bisphosphonates in experimental breast cancer bone metastasis. J Natl Cancer Inst. 2007; 99: 322–330. PMID: 17312309

40. Thudi NK, Martin CK, Nadella MV, Fernandez SA, Werbeck JL, Pinzone JJ, et al. Zoledronic acid decreased osteolysis but not bone metastasis in a nude mouse model of canine prostate cancer with mixed bone lesions. Prostate. 2008; 68: 1116–1125. doi: 10.1002/pros.20776 PMID: 18461562

41. Jeong J, Lee KS, Choi YK, Oh YJ, Lee HD. Preventive effects of zoledronic acid on bone metastasis in mice injected with human breast cancer cells. J Korean Med Sci. 2011; 26: 1569–1575. doi: 10.3346/jkms.2011.26.12.1569 PMID: 22147993

42. Luo KW, Ko CH, Yue GG, Lee MY, Siu WS, Lee JK, et al. Anti-tumor and anti-osteolysis effects of the metronomic use of zoledronic acid in primary and metastatic breast cancer mouse models. Cancer Lett. 2013; 339: 1569–1575.

43. .Bundred N. Antiresorptive therapies in oncology and their effects on cancer progression. Cancer Treat Rev. 2012; 38: 776–786. doi: 10.1016/j.ctrv.2012.02.002 PMID: 22370427

44. Guise TA, Brufsky A, Coleman RE. Understanding and optimizing bone health in breast cancer. Curr Med Res Opin. 2010; 26 Suppl.3: 3–20. doi: 10.1185/03007995.2010.533162 PMID: 21050131

45. Mundy GR. Osteoporosis and inflammation. Nutr Rev. 2007; 65: S147–151. PMID: 18240539